Empirical model for frequency content estimation of strong ground motion records of Iran

Lashgari, Ali; Jafarian, Yaser

DOI
10.1016/j.enggeo.2022.106526

Publication date
2022

Document Version
Final published version

Published in
Engineering Geology

Engineering Geology 297 (2022) 106526

Contents lists available at ScienceDirect

Engineering Geology

journal homepage: www.elsevier.com/locate/enggeo

Empirical model for frequency content estimation of strong ground motion records of Iran

Ali Lashgari [a], Yaser Jafarian [a,b,*]

[a] Geotechnical Engineering Research Center, International Institute of Earthquake Engineering and Seismology, Iran
[b] Faculty of Civil Engineering and Geosciences, Delft University of Technology (TU Delft), Netherlands

ARTICLE INFO

Keywords:
Iranian earthquakes records
Frequency-content parameter
Mean period
Ground motion prediction equation

ABSTRACT

This paper presents a new empirical model to predict the mean period (T_m) as a frequency-content parameter of earthquake record using the strong ground motions recorded in Iran during 1975–2019. An updated earthquake databank containing 2281 horizontal acceleration records was employed to develop the empirical model through a systematic fitting procedure. A simple functional form for the model was found as a function of epicentral distance (R), moment magnitude (M_w), and the shear wave velocity averaged at the top 30 m of the recording sites (V_{s30}). The proposed model is compared with three existing predictive models and the results are discussed in terms of magnitude, source-to-site, and site dependencies.

1. Introduction

The frequency content of seismic ground motions can significantly affect the seismic response of structures and geo-structures (e.g., Kramer, 1996; Rathje et al., 2004; Kumar et al., 2011; Jafarian and Lashgari, 2016). The distribution of amplitude versus different frequencies is described by the frequency content parameters (Kramer, 1996). It is well understood that civil engineering systems can potentially receive much more seismic demands when frequency-content of input motion is closer to the fundamental period of the system (Kramer, 1996; Chopra, 2001; Rathje et al., 2004).

The mean period (T_m) of an earthquake record, as a scaler frequency content parameter is commonly employed for different design purposes. Previous studies indicated that T_m as a meaningful intensity measure (IM) can provide a suitable prediction of the seismic response for the engineering systems such as structures (e.g., Kumar et al., 2011; Song et al., 2014; Bravo-Haro and Elghazouli, 2018; Hickey and Broderick, 2019) and geo-structures (e.g., Rathje and Antonakos, 2011; Rathje et al., 2014; Jafarian and Lashgari, 2017; Lashgari et al., 2020). Moreover, in recent decades, T_m is widely used to estimate the seismic-induced displacement of slopes (e.g., Rathje and Bray, 1999; Saygili and Rathje, 2008; Jafarian and Lashgari, 2016; Tsai and Chien, 2016; Jafarian et al., 2018; Lashgari et al., 2018; Macedo et al., 2020). In general, higher frequency waves could lead to shallow landslides and lower frequency shaking affects deeper areas in the slope (Bourdeau et al., 2004; Jibson and Tanyaş, 2020). Jibson and Tanyaş (2020) indicated that the mean period as a frequency content parameter is apparently the best predictor of the earthquake-induced landslide size distributions. In recent decades, T_m is widely used to develop the predictive models of seismic sliding displacement (e.g., Rathje and Bray, 1999; Saygili and Rathje, 2008; Jafarian and Lashgari, 2016; Tsai and Chien, 2016; Jafarian et al., 2018; Lashgari et al., 2018; Lashgari et al., 2021). Accordingly, prediction of T_m can play an important role to predict landslide hazard in seismic regions. T_m is calculated using the Fourier amplitude spectrum (FAS) according to Rathje et al. (1998, 2004) as follows:

$$T_m = \frac{\sum_i C_i^2 (1/f_i)}{\sum_i C_i^2} \text{ for } 0.25\ \text{Hz} \le f_i \le 20\ \text{Hz}, \text{with } \Delta f \le 0.05\ \text{Hz} \quad (1)$$

where C_i, f_i, and Δf are the Fourier amplitude coefficient, the discrete fast Fourier transform (FFT) frequencies between 0.25 and 20 Hz, and the frequency interval used in the FFT computation, respectively.

The ground-motion prediction equations (GMPEs) have been recently presented to predict IMs for design purposes (e.g., Ulusay et al., 2004; Atkinson and Boore, 2007; Campbell and Bozorgnia, 2007; Lin et al., 2011; Jafarian et al., 2014); Bastami and Soghrat, 2017; Zafarani et al., 2017; Farajpour et al., 2019). A few GMPEs have been proposed to estimate T_m although it is a valuable IM for prediction of the seismic response of an engineering system. Rathje et al. (2004) developed a

* Corresponding author at: Geotechnical Engineering Research Center, International Institute of Earthquake Engineering and Seismology, Iran.
E-mail addresses: ali.lashgarii@alum.semnan.ac.ir (A. Lashgari), yjafarianm@iiees.ac.ir (Y. Jafarian).

https://doi.org/10.1016/j.enggeo.2022.106526
Received 17 August 2021; Received in revised form 23 December 2021; Accepted 6 January 2022
Available online 10 January 2022

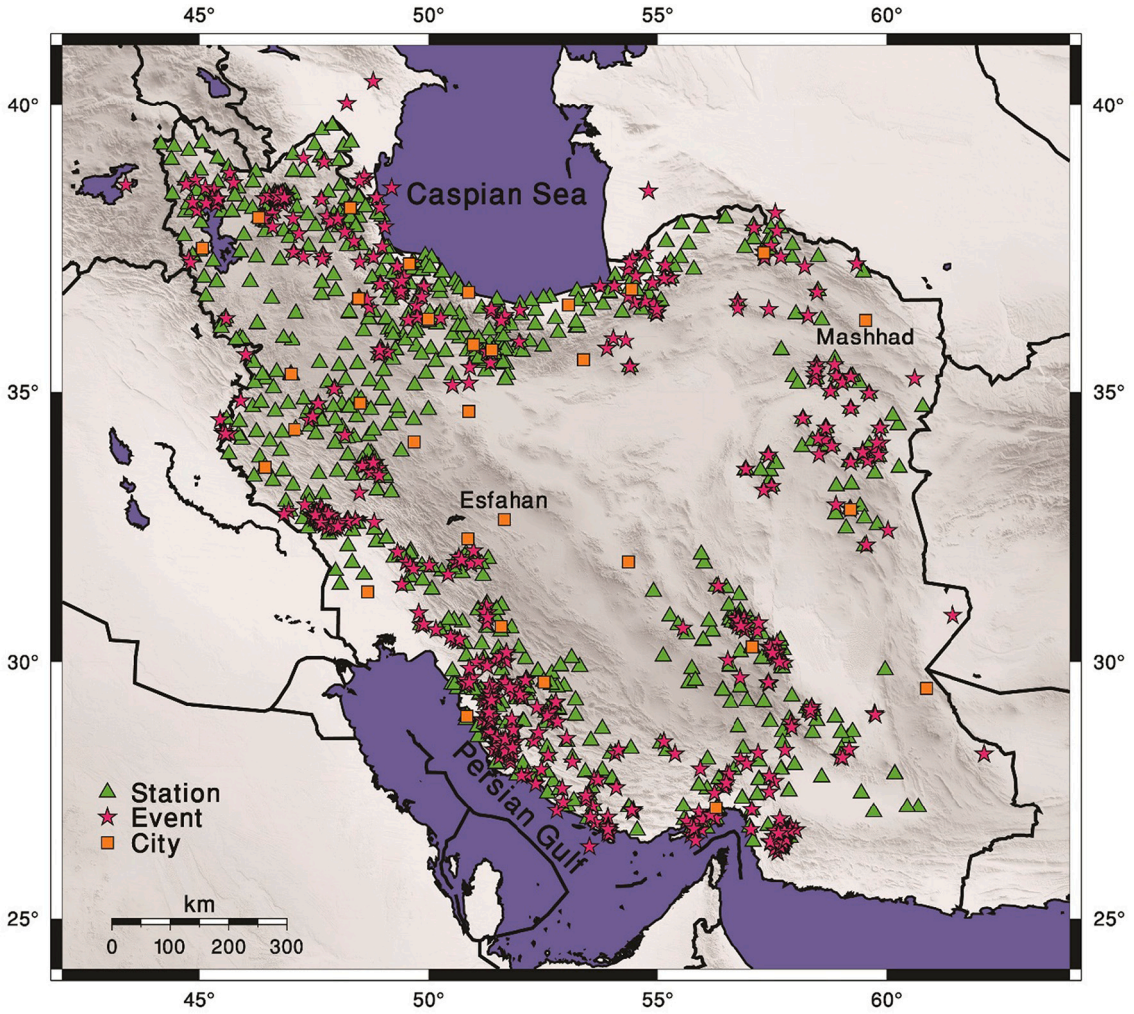

Fig. 1. Location of stations and epicenters of Iranian earthquakes records used in this study.

preceding model proposed by Rathje et al. (1998) using an extended ground motion database and predictor variables. Yaghmaei-Sabegh (2015) proposed an empirical model using several Iranian earthquake ground motions. A database of global earthquake ground motions was employed by Du (2017, 2019) to develop a predictive model for T_m. Chousianitis et al. (2018) presented a model for T_m prediction using the earthquake data recorded in Greece.

Iran has been recognized as a tectonically active region in the world. A large database of earthquake ground motions has been compiled by Road, Housing, and Urban Development Research Center (BHRC) of Iran. Iran is exposed to spread phenomena of landslides, especially in the Alborz-Azerbaijan and Zagros mountains (Jafarian et al., 2019). There are numerous structures (e.g., buildings) and geostructures (e.g., slopes) located in Iran that are often exposed to seismic hazards such as earthquake-induced landslides. Development of predictive models for T_m based on the ground motions recorded in Iran could lead to more desirable estimation of seismic and geotechnical hazards.

In the current study, a new predictive model is presented to estimate $T_m$in Iran plateau based on a large database of earthquake ground motion accelerations recorded in this seismic region. The collection of Iran's earthquake records employed in the current study is primarily presented in this paper. Subsequently, the predictive model of $T_m$is generated by the systematic multiple regression analysis as a simple function of the epicentral distance (R), the shear wave velocity at top of 30 m (V_{s30}), and the moment magnitude (M_w). Finally, performance of the model is evaluated by the parametric study and comparison with a regional-scale and two global-scale models.

2. The strong Motion Dataset

The Iran plateau is compressed by the Arabian and Eurasian tectonic plates. The tectonic activities of the Iran plateau were mainly controlled by the convergence of the Arabian and Eurasian plates that leads to moderate to large shallow crustal earthquakes by the strike-slip and reverse faults (e.g., Berberian, 2014; Zafarani and Soghrat, 2017). The recent Sarpol-e Zahab earthquake (2017, $M_w = 7.3$) triggered significant damages in the western of Iran where the Arabian and Eurasian plates collide (Zafarani et al., 2020).

The Iranian Strong Motion Network (ISMN) which is now part of BHRC was established in 1973 to record earthquake input motions by installing of recording stations. More than 10,000 three-component time series of acceleration, which includes a pair of horizontal acceleration and one vertical acceleration components, were recorded by ISMN in Iran during 1975–2013 (Zafarani and Soghrat, 2017). Moreover, more than 1700 three-component time series of acceleration were recorded by more than 833 stations during 2013–2019. In this study, an extended database of the ground motion records from ISMN (including 1975–2019 acceleration records) was employed to develop an empirical model for T_m. The database was composed of 4562 accelerations records of two horizontal components (H1 and H2) associated with 536 earthquakes occurred during 1975–2019. The locations of stations and events were shown in Fig. 1. The multi-resolution wavelet analysis (Ansari

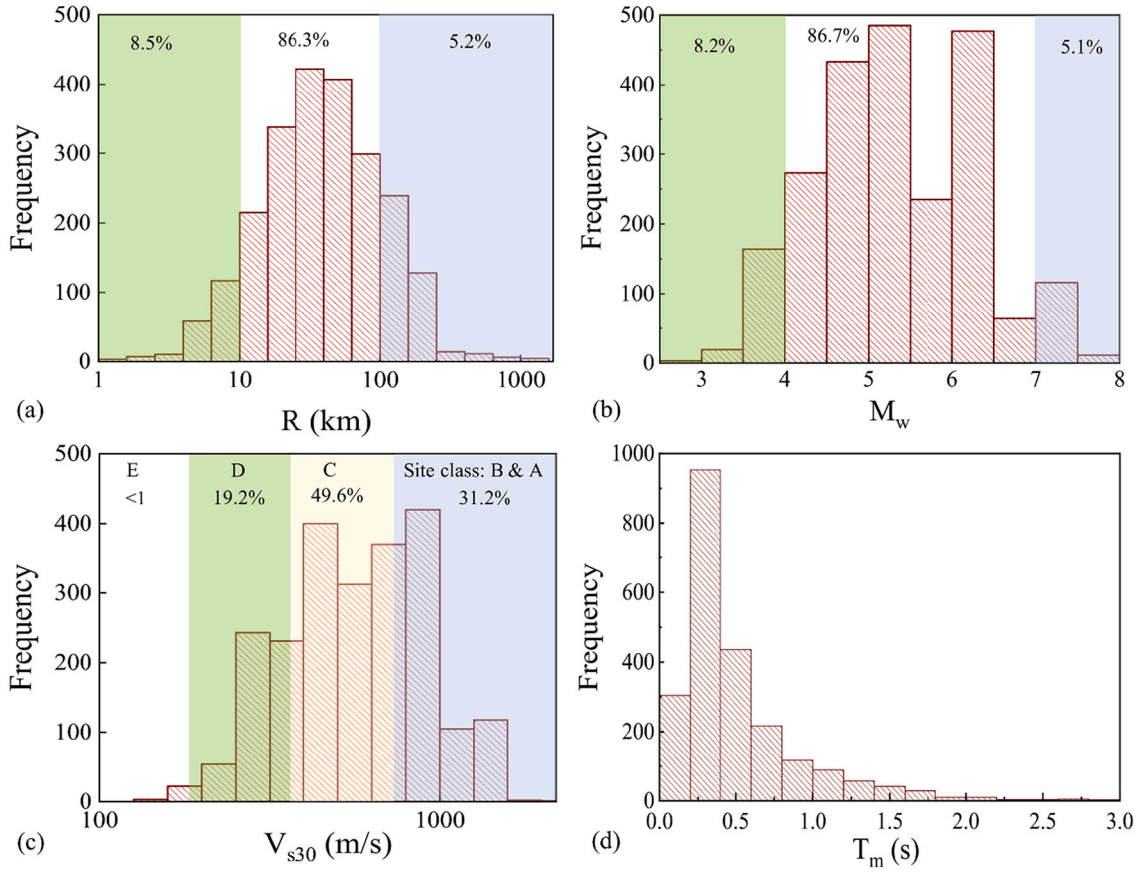

Fig. 2. Histograms of 2281 Iranian earthquake records database for (a) epicentral distance R; (b) moment magnitude M_w; (c) shear wave velocity V_{s30}; (d) mean period, T_m.

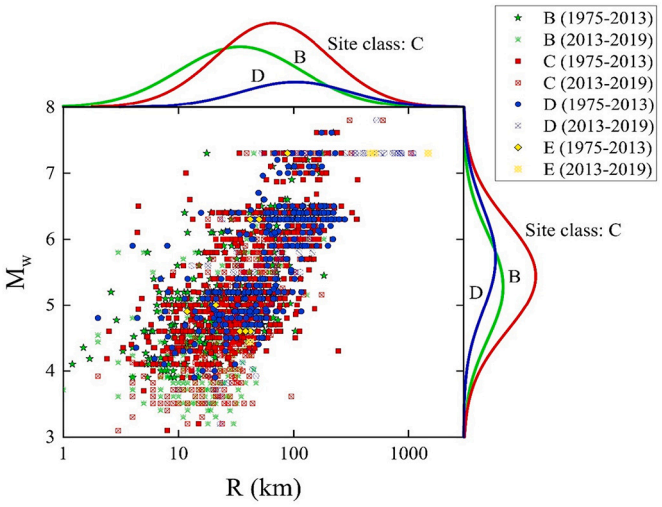

Fig. 3. Distribution of R and M_w of 2281 used ground motions.

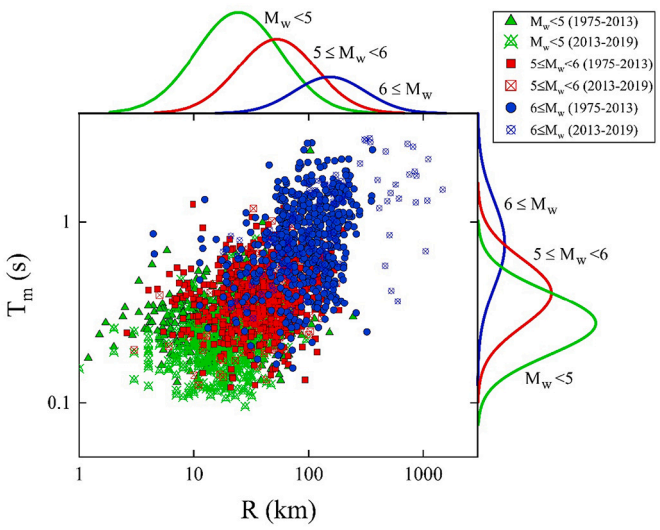

Fig. 4. Distribution of T_m and R of 2281 used ground motions.

et al., 2010) was used to eliminate unsuitable noise from the earthquake records. This analysis was also employed by Zafarani and Soghrat (2017) for the filtering of the Iranian earthquake records. Moreover, the baseline correction was made for all used records. The Euclidean norm of the of T_ms ($\sqrt{{T_{m,H1}}^2 + {T_{m,H2}}^2}$) were used for each pair of horizontal components (H1 and H2) because the Fourier transform space is a vector space (Rathje et al., 2004). Finally, one $T_m$was obtained for one station in one event. However, the averaging method in this study is different from the approach used by Rathje et al. (2004) who employed combination of Fourier spectrums of two components to calculate T_m. Geometric mean was also employed by other researchers such as Chousianitis et al. (2018) to estimate averaged T_m. The current model is presented for the prediction of the Euclidean norm of the horizontal components of T_m.

The different source-to-site distances such as Joyner-Boore (R_{jb}),

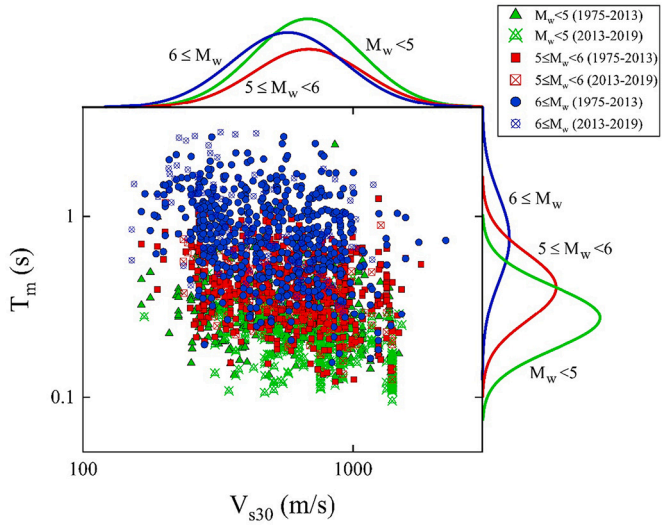

Fig. 5. Distribution of T_m and V_{s30} of 2281 used ground motions.

rupture (R_{rub}), hypocentral (R_{hyp}), and epicentral (R) distances are employed to develop GMPEs, each one has advantages and disadvantages. $R_{jb}$and $R_{rub}$are measured on the basis of the fault geometry and the rupture plane and can lead to a more accurate GMPE. The R and R_{hyp}-based GMPEs can be used to estimate the ground-motion field when only the epicentral location has been determined immediately following an earthquake (Bommer and Akkar, 2012). The lack of detailed information about fault geometry and the rupture plane for most earthquakes in Iran prevented the use of R_{jb}or R_{rub}in this study. However, the authors acknowledge that $R_{jb}$and $R_{rub}$are a crucial need for the development of an accurate model. Based on Chousianitis et al. (2018), R_{hyp} was not used to avoid bias due to poorly resolved focal depths. Accordingly, R was employed to develop the predictive model in this study.

The low-frequency components of seismic waves can be amplified

Table 1
The values of "a" coefficients and the results of the regression [Eq. (2)].

V_{s30}(m/s)	Coefficient	$M_w < 5$	$5 \le M_w < 6$	$6 \le M_w < 7$	$7 \le M_w$
$V_{s30} < 360$	a_1	−1.477	−1.3447	−1.04	−0.9257
	a_2	−0.979	−0.9745	−0.9677	−0.9706
	SE	0.035	0.043	0.044	0.061
	RSE (%)	0.032	0.034	0.038	0.109
$360 \le V_{s30} < 560$	a_1	−1.7316	−1.6554	−1.0674	−1.0816
	a_2	−0.9633	−0.9598	−0.9716	−0.9697
	SE	0.029	0.011	0.021	0.005
	RSE (%)	0.011	0.006	0.014	0.014
$560 \le V_{s30} < 760$	a_1	−1.7756	−1.6082	−1.301	0.0889
	a_2	−0.973	−0.9688	−0.9678	−1.0157
	SE	0.011	0.022	0.019	0.028
	RSE (%)	0.006	0.013	0.016	0.155
$760 \le V_{s30}$	a_1	−1.8366	−1.9018	−1.4409	−1.6235
	a_2	−0.9693	−0.9572	−0.9646	−0.9518
	SE	0.028	0.029	0.024	0.108
	RSE (%)	0.008	0.013	0.021	0.597

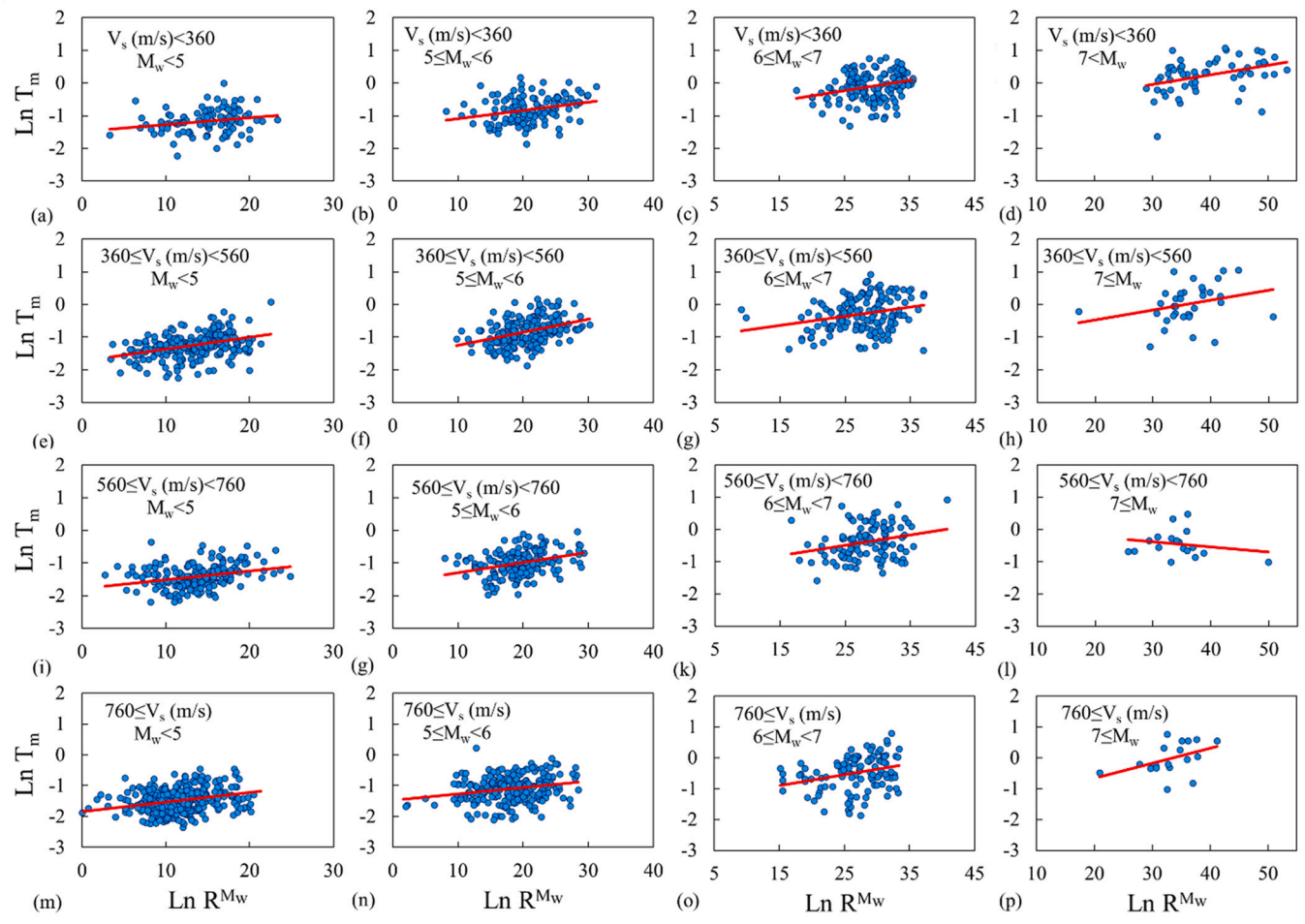

Fig. 6. Variations of $T_m$versus $R^{M_w}$and the proposed model [Eq. (2)] for different classes of shear wave velocity and moment magnitude.

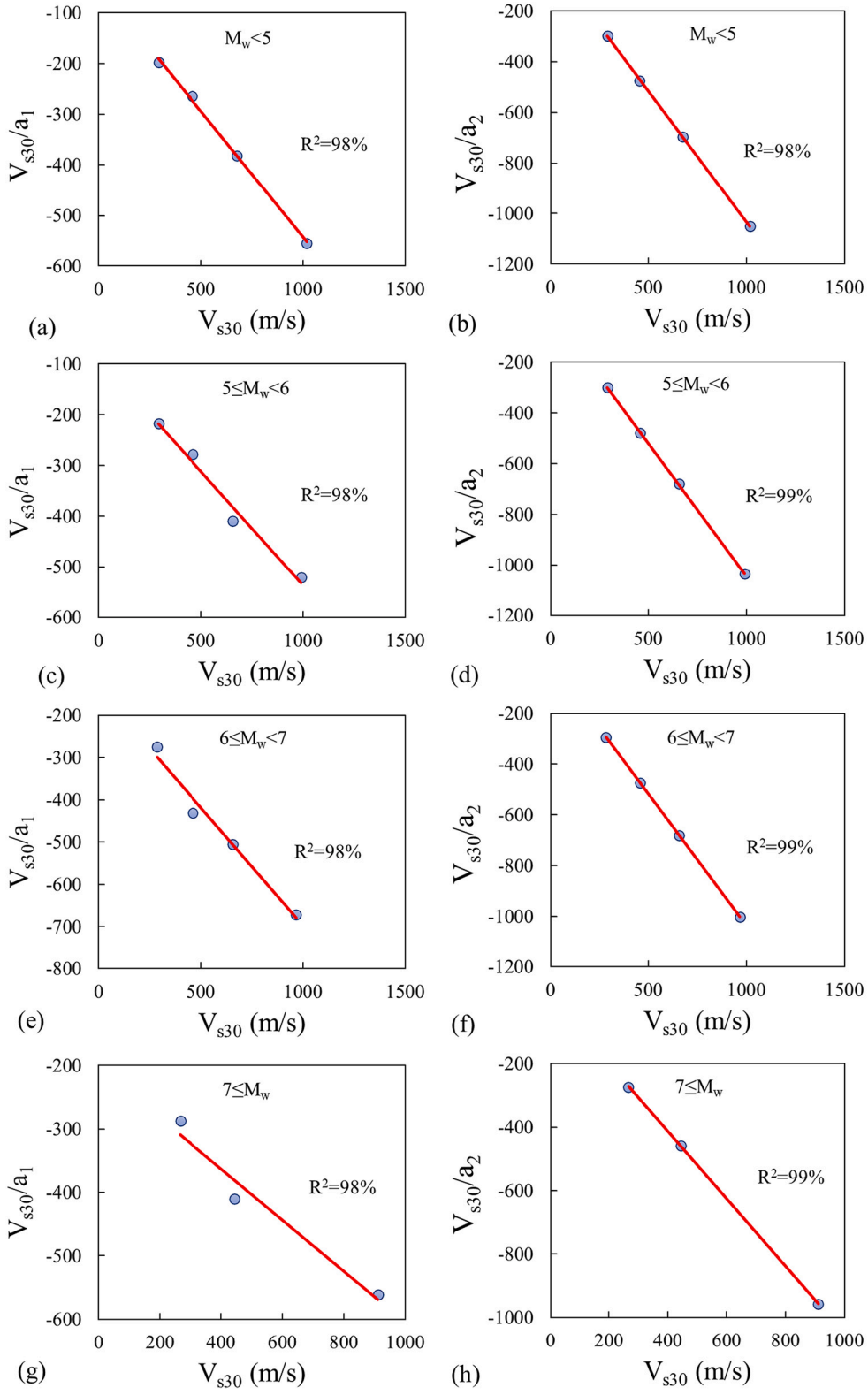

Fig. 7. The "a" fitting coefficients with respect to the variations of shear wave velocity for various moment magnitudes.

due to the resonance effect within soil layers. This phenomenon can significantly affect the frequency content of input motions (Du, 2017). Accordingly, T_m as a frequency content parameter is influenced by site conditions. The local site conditions are represented by V_{s30} on the GMPEs. This parameter can help to investigate the resonance phenomena of a site. However, the use of V_{s30} alone for the site effect assessment could be challenging, since the shear wave is tied to soil rigidity (Castellaro et al., 2008). The site classification is generally used to evaluate the local site effect on the GMPEs by the values of V_{s30} according to the standards or guidelines criteria (e.g., Eurocode, NEHRP). However, new approaches have been recently proposed for site classification which can better show the site effects (e.g., Kotha et al., 2018; Del Gaudio et al.,

Table 2
The values of "a" coefficients and the results of regression [Eqs. (3–4)].

"a" coefficient	Coefficient	$M_w < 5$	$5 \le M_w < 6$	$6 \le M_w < 7$	$7 \le M_w$
a_1	b_1	−45.192	−87.254	−140.14	−201.47
	b_2	−0.4977	−0.4483	−0.5575	−0.4038
	SE	0.028	0.003	0.043	0.037
	RSE (%)	0.695	0.077	1.086	1.242
a_2	b_3	1.3471	6.7902	3.0412	10.31
	b_4	−1.0328	−1.0498	−1.039	−1.0611
	SE	0.003	0.0001	0.002	0.004
	RSE (%)	0.081	0.004	0.059	0.145

2019).

The frequency content of the ground motion can be affected by the focal mechanism of the events (e.g., Rathje et al., 2004). Previous studies show that normal faulting causes higher amplitude/Tm values than strike-slip or thrust faulting (e.g., Zhao et al., 2016; Chousianitis et al., 2018). However, different GMPEs were developed for unknown focal mechanisms (e.g., Chousianitis et al., 2018; Xu et al., 2019). The focal mechanism is not considered in this study since the focal mechanisms were not presented in detail in the database of Iranian strong motion records.

The histograms of R, M_w, V_{s30}, and T_m of the used ground motion database are shown in Fig. 2. Fig. 2(a) shows that the epicentral distances of 5.2% of the records are greater than 150 km, 86.3% fall between 10 and 150 km, and more than 8% of the records are smaller than 10 km. Fig. 2(b) demonstrates that the moment magnitude (M_w) of more than 8% of the records are smaller than 4, 86.7% are between 4 and 7, and 5.1% are greater than 7. Moreover, the variations of V_{s30} of station sites are shown in Fig. 2(c). The V_{s30} values of 1621 records were reported by BHRC while V_{s30} values of 660 records are not available. Accordingly, the value of V_{s30} was estimated for these stations using the presented method by Wald and Allen (2007) and Allen and Wald (2009). Wald and Allen (2007) presented a methodology for deriving maps of V_{s30}anywhere in the world using topographic slope as a proxy. A global V_{s30} map server was provided by The U.S. Geological Survey (USGS) earthquake hazard program (https://earthquake.usgs.gov/data/vs30/) based on Wald and Allen (2007) and Allen and Wald (2009)'s models. The values of $V_{s30}$are taken into account as the local site condition in this study by soil categorization released by the standards of National Earthquake Hazards Reduction Program (NEHRP). As shown in Fig. 2 (c), less than 1% of records fall in site class E (soft soil, $V_{s30} < 180$ m/s), 19.2% in site class D (stiff soil, $180 \le V_{s30} < 360$ m/s), 49.6% in site class C (very dense soil and soft rock, $360 \le V_{s30} < 760$ m/s), and 31.2% in site classes B (rock, $760 \le V_{s30} \le 1500$ m/s) and A (hard rock, 1500 m/s $\le V_{s30}$). Fig. 2(d) indicates that the values of $T_m$variate in different ranges between 0 and 3 s. However, its average is about 0.25 s.

The distribution of $M_w$was plotted with respect to the epicentral distances of the earthquake records database per different site classes in Fig. 3. The strong ground motion records are separated based on the recording dates for two ranges between 1975 and 2013 and 2013–2019 in Fig. 3. It demonstrates that the average moment magnitude is about 5, 5.3, and 5.9 for the recorded earthquakes in the site classes B, C, and D, respectively. Moreover, the average epicentral distance is about 40, 59, and 107 km for the recorded earthquakes in the site classes B, C, and D, respectively. As shown in this figure, the average moment magnitude in the database is around 5.5 while the average epicentral distance is about 63 km.

The variations of $T_m$were plotted versus the epicentral distances for three levels of magnitude such as low, moderate, and high in Fig. 4. The strong ground motion records are distinguished on the basis of the recording dates in Fig. 4. As shown in this figure, the value of $T_m$decreases when $M_w$or R decreases. The average value of $T_m$is about 0.28, 0.42, and 0.91 s for $M_w < 5$, $5 \le M_w < 6$, and $M_w \ge 6$, respectively. Fig. 4 shows that the epicentral distance of data is around 24, 47, and 127 km

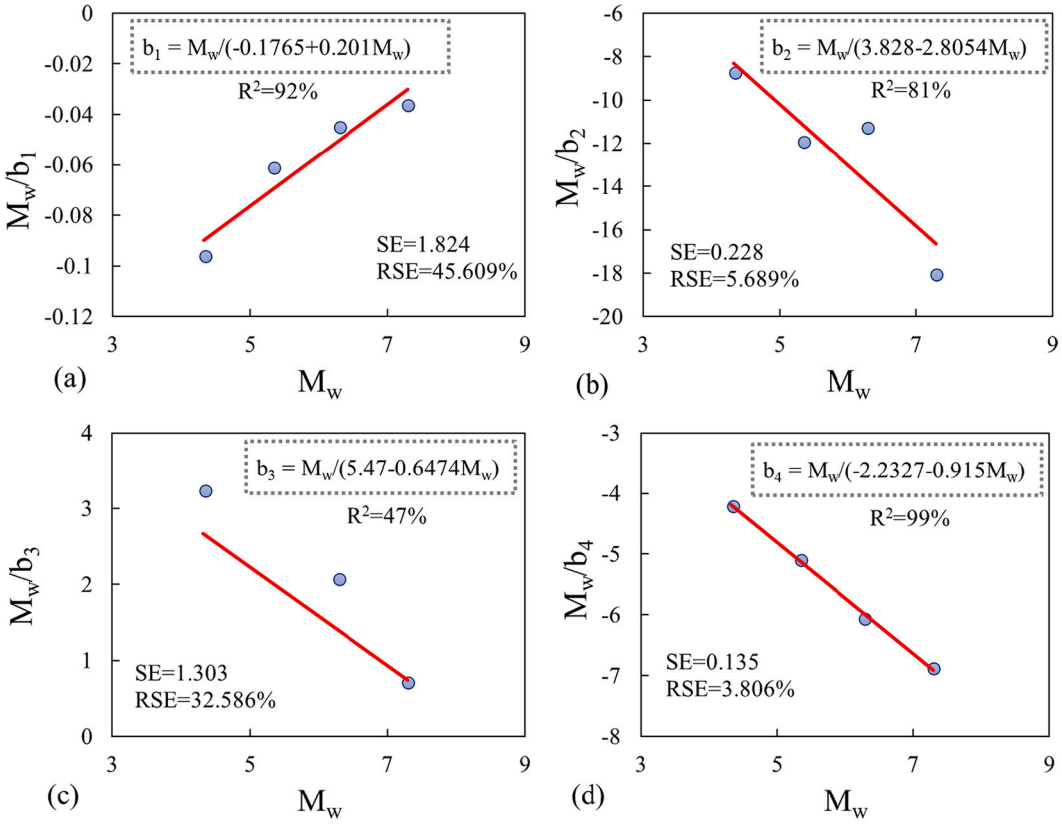

Fig. 8. The "b" coefficients plotted versus various M_w.

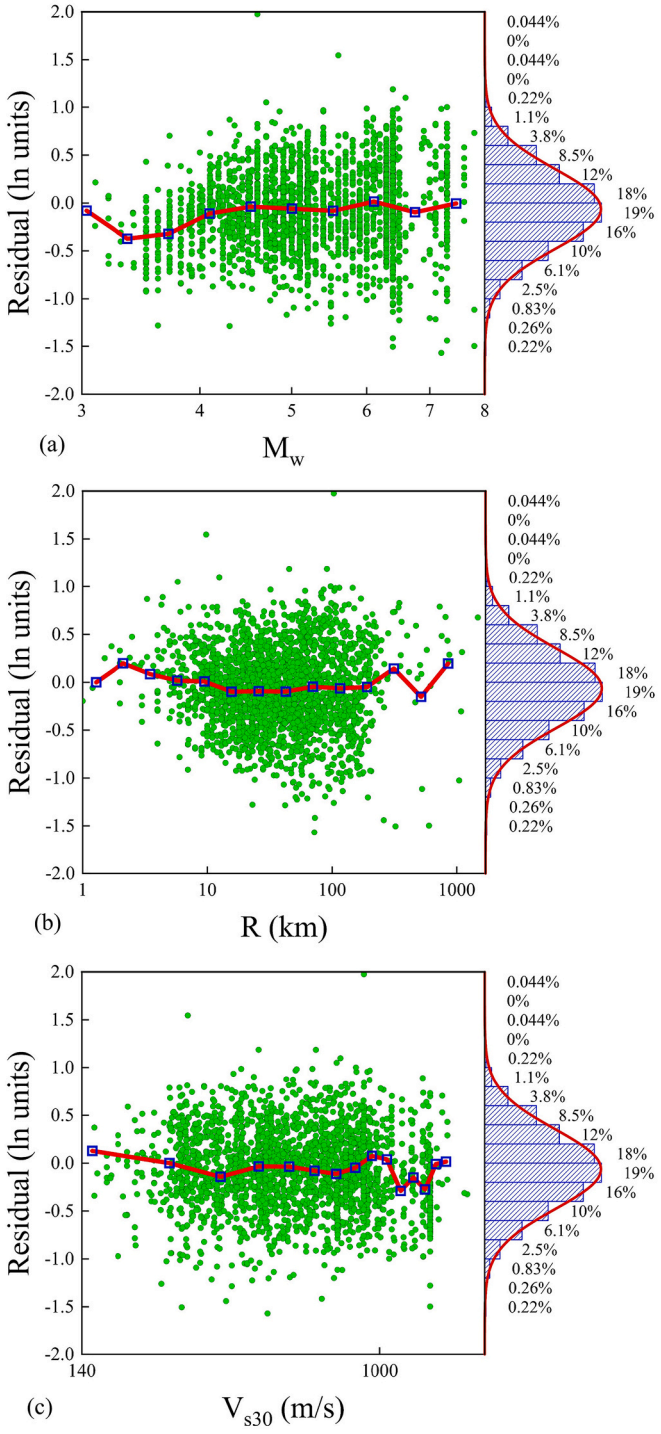

Fig. 9. Residuals of the proposed model (Eq. [2]) with respect to (a) M_w; (b) R; (c) V_{s30}.

for $M_w < 5$, $5 \leq M_w < 6$, and $M_w \geq 6$, respectively.

Fig. 5 shows the variations of $T_m$versus $V_{s30}$for three levels of magnitude. As shown in this figure, there is a meaningful relationship between the variations of T_m, V_{s30}, and M_w. Fig. 5 indicates that the value of T_m decreases when V_{s30} increases for all levels of magnitude. Moreover, the value of T_m increases with the magnitude in a constant V_{s30}.

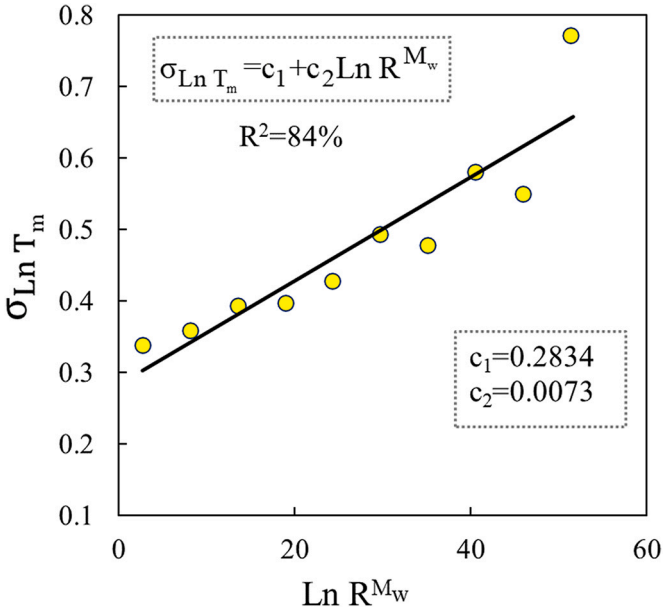

Fig. 10. Variation of $\sigma_{Ln\ Tm}$versus variations of Ln $R^{M_w}$for the proposed predictive model [Eq. (2)].

3. The predictive model of T_m

The mean period as a frequency content parameter can be affected by the magnitude, distance, focal mechanism, and site shear wave velocity. Accordingly, most presented models were developed based on these parameters (e.g., Rathje et al., 1998). The evaluation of the GMPEs shows that the models are generally functions of site effect, the magnitude and focal mechanism (e.g., Rathje et al., 2004; Yaghmaei-Sabegh, 2015; Du, 2017; Chousianitis et al., 2018). The combination of these parameters can provide an accurate model for prediction of T_m. However, simultaneous attention to accuracy and simplicity can increase the applicability of the model for engineering purposes. In this study, three parameters comprising the epicentral distance, the moment magnitude, and site shear wave velocity were nominated to generate the model of T_m.

The former studies of authors demonstrated that the data classification per small ranges of parameters can decrease the scattering of data and increase the correlation coefficient in a regression analysis (e.g., Lashgari et al., 2018; Jafarian et al., 2019). Accordingly, the correlations between T_m and relative parameters were investigated for some small ranges of M_w within each site class.

Different functional forms were evaluated in each data class to achieve the optimum functional form. Finally, the best model was chosen based on three criteria: (1) the physical concept of Tm; (2) the simplicity to increase the applicability of the model, (3) the accuracy by consideration of the model residuals. These selection criteria are commonly used to choose the most appropriate functional forms (e.g., Du, 2017). Moreover, the value of R-squared (R^2), the relative standard error (RSE), and the standard error (SE) were used to assess efficiency of the functional forms. The regression procedure is performed on the basis of the linear regression process which takes the best functional form as follows:

$$Ln\ T_m = a_1 + (1 + a_2) Ln\ R^{M_w} \pm \sigma_{Ln\ T_m} \quad (2)$$

whereT_m, a_1 and a_2, R, M_w, and $\sigma_{Ln\ T_m}$are the mean period in second, the constant coefficients as a function of the moment magnitude and shear wave velocity, the epicentral distance in km, the moment magnitude, and the standard deviation of the proposed model, respectively.

The data of T_m were plotted versus Ln $R^{M_w}$for several categories of

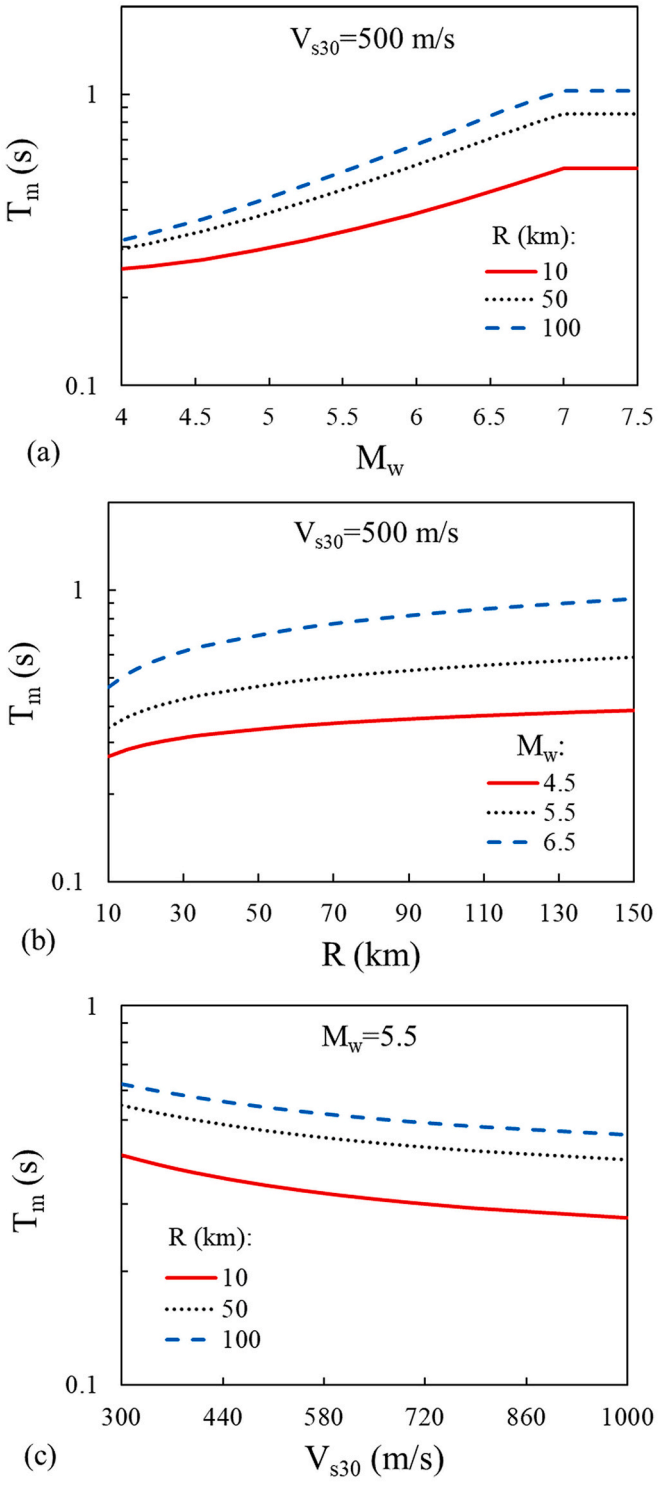

Fig. 11. Variations of the predicted values of $T_m$versus the variations of (a) M_w; (b) R; (c) V_{s30}.

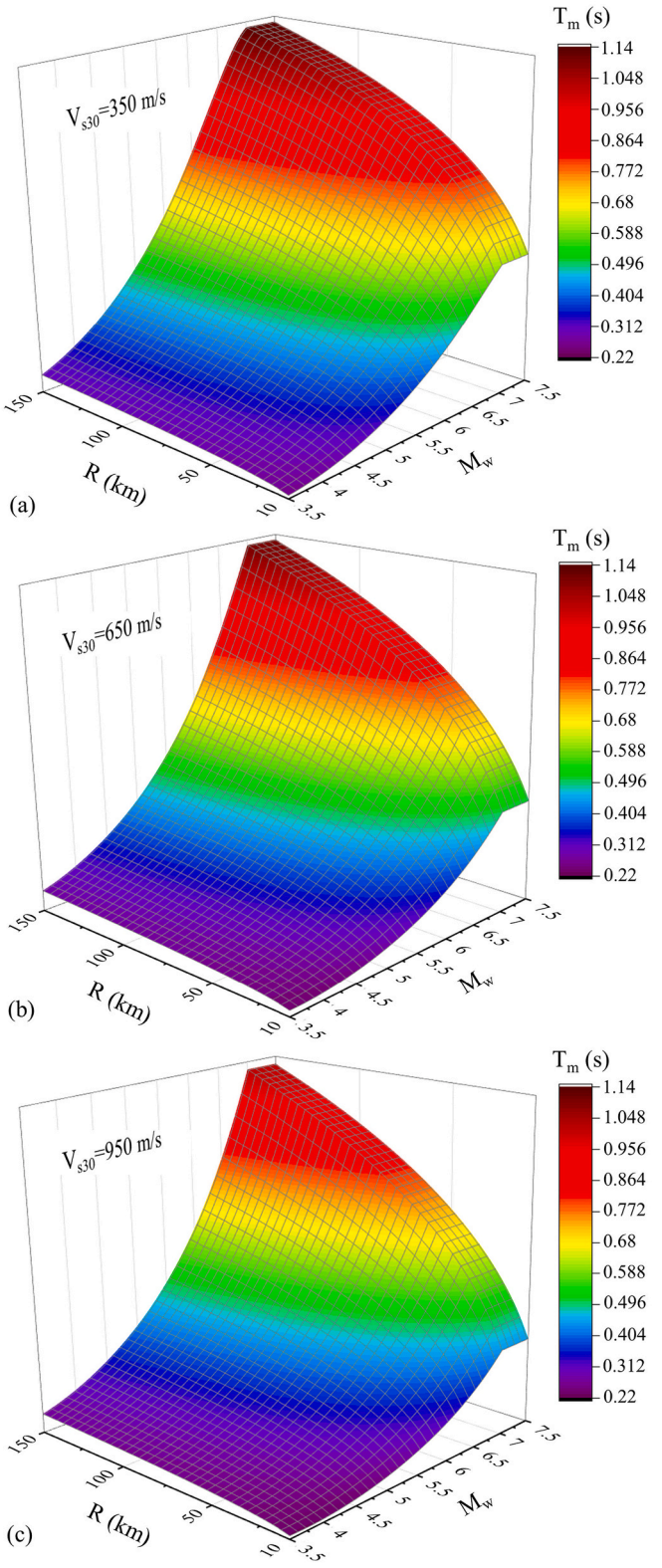

Fig. 12. 3D plot of the variation of $T_m$versus the variations of $M_w$and Rfor (a) V_{s30} = 350 m/s; (b) V_{s30} = 650 m/s; (c) V_{s30} = 950 m/s.

site classes and three levels of magnitude in Fig. 6. The moment magnitude was classified into four levels of magnitude including low ($M_w < 5$), moderate ($5 \leq M_w < 6$), high ($6 \leq M_w < 7$) and very high ($M_w \geq 7$) for regression analyses. The predictive model [Eq. (2)] was individually fitted for each category of V_{s30} and M_w to obtain "a" coefficients by the multiple regression procedure. As shown in Figs. 4-5, the recorded data follow a reasonable trend versus the variations of $V_{s30}$and R when M is divided into different classes. Accordingly, the data were categorized into four groups of M and V_{s30}. The "a" coefficients as a function of V_{s30} and M_w were calculated for all data groups. The effect of parameter variations can be appropriately evaluated in a predictive model by multiple regression procedures (Lashgari et al., 2018; Jafarian

Table 3
Summary of the presented predictive models for T_m(after Du, 2017).

Model	Range of M_w	Range of R (km)	Input parameters	Number of records	Earthquake records
Rathje et al. (1998)	[5.2–7.3]	[1−200]	M_w, R_{rup}	306	World
Rathje et al. (2004)	[4.9–7.6]	[0.2–200]	M_w, R_{rup} S_c, S_d, FD	835	World
Yaghmaei-Sabegh (2015)	[3.7–7.7]	[0.7–293]	M_w, R_{rup}, S_c, S_d	575	Iran
Du (2017)	[3.05–7.9]	[0.1–499.5]	M_w, R_{rup}, V_{s30}, I_{dir}, Z_1, Z_{tor}	8491	World
Chousianitis et al. (2018)	[4–6.8]	[0.3–200]	M_w, R S_c, S_d, FM	652	Greece
This study	[2.9–7.8]	[1–1477]	M_w, R, V_{s30}	2281	Iran

M_w: moment magnitude; R_{rup}: closest distance from the site to the rupture plane; R: horizontal distance from the site to the epicenter; S_c and S_d: indicators of site class; FD and I_{dir}: indicators of the directivity effect; V_{s30}: time-average shear wave velocity of the upper 30 m (m/s); Z_1: depth to the 1.0 km/s shear wave isosurface (km); Z_{tor}: depth to the top of rupture (km); FM: fault mechanism.

et al., 2019; Lashgari et al., 2021).

It is noted that the constant coefficients are supposed as a function of M, R, and V_{s30} in this study. However, Eq. (2) represents a basic form as a function of M and R and it was expected that the coefficients were supposed to only be dependent on V_{s30}. The correlation between the coefficients and V_{s30} was firstly investigated without classifications of M. Despite many efforts, a reasonable relationship was not found to describe the correlation between the variations of the coefficients versus V_{s30}.

The "a" coefficients (a_1 and a_2), the relative standard error (RSE), and the standard error (SE) were shown in Table 1 for each class of V_{s30} and M_w. The evaluation of the "a" coefficients indicates that they have a clear correlation with the variations of V_{s30}in a constant site class and different categories of M_w. Accordingly, the $T_m$values were classified into four groups of V_{s30} for each class of moment magnitude.

The distribution of the "a" coefficients was plotted with respect to the variation of V_{s30} per four magnitude classes in Fig. 7. The values of V_{s30} are an average of V_{s30} data for each magnitude class. As shown in Fig. 7, a correlation can be found to predict the "a" coefficients based on the variations of the shear wave velocity or $M_w < 5$, $5 \le M_w < 6$, $6 \le M_w < 7$, and $M_w \ge 7$. A regression process was performed to assess a suitable prediction of the "a" coefficients. It is noted that the data of the third class ($7 \le M_w$ and $560 \le V_{s30}$(m/s) < 760) is not considered in the regression analysis since the number of data is low in this class. Eqs. (3–4) are recommended to estimate the "a" coefficients:

$$a_1 = V_{s30}/(b_1 + b_2 V_{s30}) \tag{3}$$

$$a_2 = V_{s30}/(b_3 + b_4 V_{s30}) \tag{4}$$

where "b" coefficients (b_1, b_2, b_3, and b_4) are dependent on the moment magnitude as the variable factors. The values of "b" coefficients, SE, and RSE were shown in Table 2.

Fig. 8 represents the values of the "b" coefficients were plotted against the variations of M_w, indicating that the "b" coefficients have a strong correlation with M_w. The best-fit equations form between the "b" coefficients and the moment magnitude are presented as follows:

$$b_1 = M_w/(-0.1765 + 0.201M_w) \tag{5}$$

$$b_2 = M_w/(3.828 - 2.805M_w) \tag{6}$$

$$b_3 = M_w/(5.47 - 0.6474M_w) \tag{7}$$

$$b_4 = M_w/(-2.2327 - 0.915M_w) \tag{8}$$

where M_w is moment magnitude. The values of SE and RSE of Eqs. [5–8] were shown in Table 2. It is noted that a theoretical magnitude cut-off at 7 was used for $T_m$model owing the fact that there is no magnitude dependence at large magnitudes where the corner frequency is outside the frequency range used for the T_m computation (Rathje et al., 2004). Accordingly, the added low-frequency energy generated by large earthquakes cannot affect T_m (Rathje et al., 2004; Yaghmaei-Sabegh, 2015). More details on the theoretical magnitude cut-off can be found in Rathje et al. (2004), Brune (1970), and Du (2017). The magnitude cut-off values as 7.25, 7.25, and 7.3 were applied in the magnitude term by Rathje et al. (2004), Yaghmaei-Sabegh (2015), and Du (2017), respectively. Therefore, the magnitude of 7 was assumed as a cut-off level in the proposed model when M_w is greater than 7.

The sufficiency condition of the input parameters of the empirical model is evaluated by the residuals (i.e., $LnT_{m,\ observed}$ - $LnT_{m,predicted}$) to demonstrate whether the model has bias for the input parameters (e.g., Karimi and Dashti, 2017; Lashgari et al., 2018; Lashgari et al., 2020). Figs. 9(a-c) show the variations of the residuals with respect to input parameters of the proposed model including M_w, R, and V_{s30}. The average lines of the residuals shown by the square symbol in Fig. 9 were calculated in each series of input parameters. As shown in Fig. 9, more than 65% of the residuals fall between ±0.5. Fig. 9(a) demonstrates that the average line of residuals is around zero for the most part of M_w. However, lack of data has led to increased residuals for the data in the range of $M_w < 4$. The multiple regression analysis needs to have enough data in each data group in order to achieve a suitable accuracy. However, Fig. 9(a) confirms that there is a rare amount of data with $M_w < 4$, in fact, the amount of data is not adequate for each class of V_{s30}. The number of data is 14 for $V_{s30} < 360$and 38 for $360 < V_{s30} < 360$ and $560 < V_{s30} < 760$. In addition, it might be due to the characteristics of small earthquakes. The ground motions of small earthquakes may be sensitive to differences in crustal structure and crustal stress states (Atkinson and Morrison, 2009; Chiou et al., 2010). It is noted that the evaluation of low magnitude ground motions was not the purpose of this study due to the lack of enough data recorded in Iran. Accordingly, the model must be employed with caution for small earthquakes. Fig. 9(b) shows that the average line of residuals is around the zero line, on the contrary to $R >$ 150 km. Fig. 9(c) demonstrates that the average line of residuals is close to zero when the shear wave velocity is greater than 200 m/s and less than 1000 m/s.

The errors of the model ($T_{m,\ observed}$ - $T_{m,\ predicted}$) in natural log units were classified into ten small ranges of $R^{M_w}$to calculate the standard deviation of the model ($\sigma_{Ln\ T_m}$). The values of $\sigma_{Ln\ T_m}$were shown versus Ln R^{M_w} by yellow dots in Fig. 10, which illustrates the values of $\sigma_{Ln\ T_m}$with respect to Ln R^{M_w}. The value of $\sigma_{Ln\ T_m}$is less than 0.5 for Ln $R^{M_w} <$ 40.

The framework of the predictive model of T_m is summarized in the following equations:

$$\begin{aligned} &Ln\ T_m = a_1 + (1 + a_2) Ln\ R^{M_w} \pm \sigma_{Ln\ T_m} \quad \text{for } M_w \le 7 \\ &\sigma_{Ln\ T_m} = 0.2834 + 0.0073 Ln\ R^{M_w} \end{aligned} \tag{9a}$$

in which

$$a_1 = \frac{V_{s30}}{[M_w/(-0.1765 + 0.201M_w)] + [M_w/(3.828 - 2.805M_w)]V_{s30}} \tag{9b}$$

$$a_2 = \frac{V_{s30}}{[M_w/(5.47 - 0.6474M_w)] + [M_w/(-2.2327 - 0.915M_w)]V_{s30}} \tag{9c}$$

The moment magnitude of 7 ($M_w = 7$) was assumed in Eq. (9) for M_w

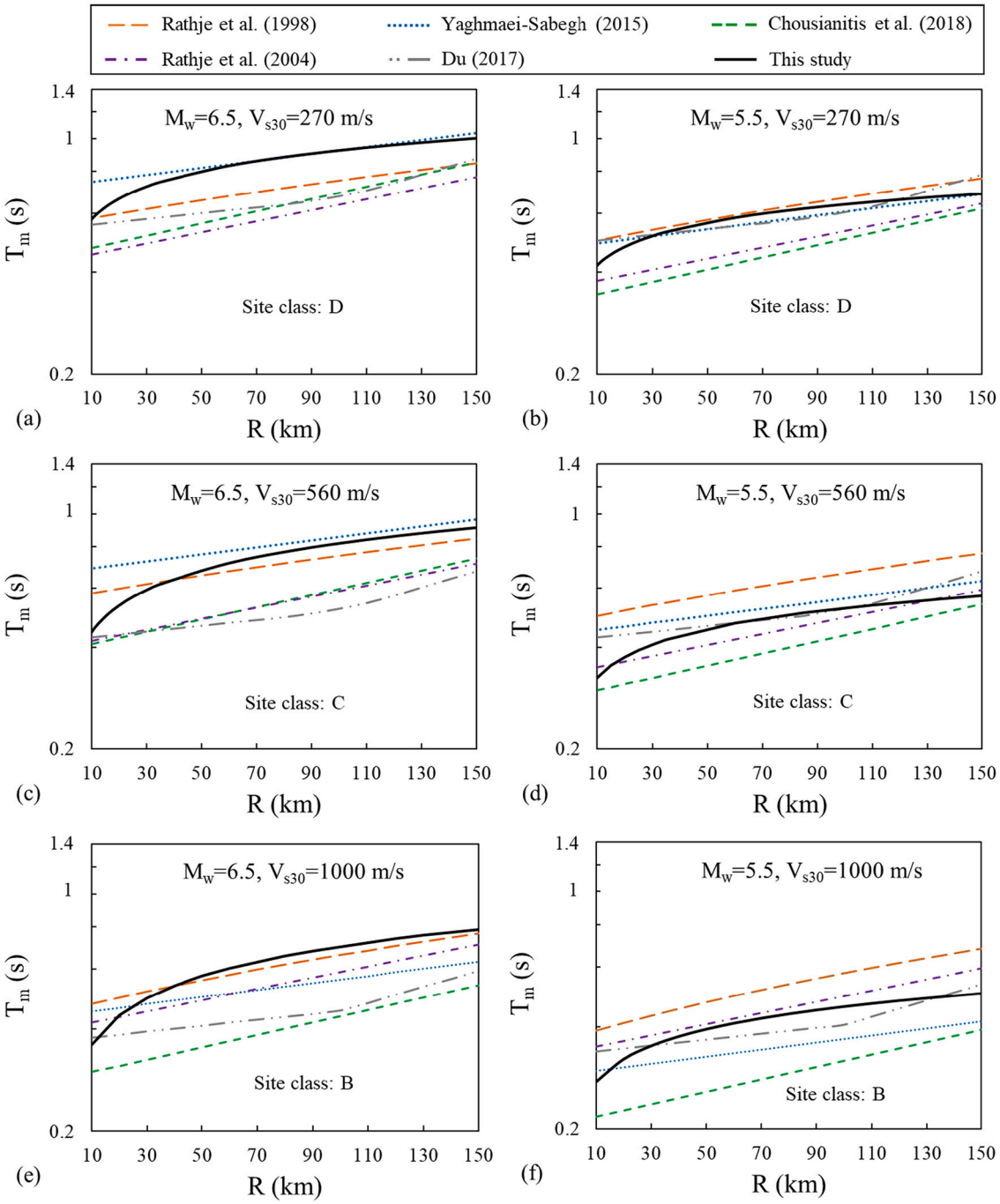

Fig. 13. Comparison of the values of T_m versus R predicted by the current model with the previous models for (a) Site class D,V_{s30} = 270 m/s, M_w = 6.5; (b) Site class D, V_{s30} = 270 m/s, M_w = 5.5; (c) Site class C, V_{s30} = 560 m/s, M_w = 6.5; (d) Site class C, V_{s30} = 560 m/s, M_w = 5.5; (e) Site class B, V_{s30} = 1000 m/s, M_w = 6.5; (f) Site class B, V_{s30} = 1000 m/s, M_w = 5.5.

> 7. A simple C#-based tool was written for possible application of the model. This tool is presented as the supplemental data. As shown in Figs. 3-5, the available data do not uniformly cover all ranges of input parameters M_w, R, and V_{s30}. For example, there is not fairly amount of data within $6.5 < M_w < 7$ or $R > 200$ km. Therefore, applicability of the proposed model might be limited in these ranges and the model has to be improved in the future.

4. Model evaluation and comparison

The variation of the predicted values of the proposed model [Eq. (9)] were plotted versus the input variable variation of M_w, R, and V_{s30} in Figs. 11(a-c). Fig. 11(a) indicates that the $T_m$follows an increasing trend for different distance when moment magnitude increases. The difference of $T_m$with increasing of $M_w$so that it is around 1.25 times for $R = 10$ and $R = 100$ km in $M_w = 4$ and 1.85 in $M_w = 7$. Fig. 11(b) indicates that the$T_m$values increase at different levels of magnitude when the epicentral distance changes. However, its increasing trend declines for R > 50 km. Fig. 11(c) shows that the variation of V_{s30} has exponentially affected the mean period. $T_m$decreases with increasing of V_{s30}so that it decreases around 1.35 times when V_{s30}enhances from 300 to 1000 m/s given a constant distance.

Figs. 12(a–c) indicate 3D plots of $T_m$with the values of M_w and R for different values of V_{s30} including 350, 650, and 950 m/s. These plots can

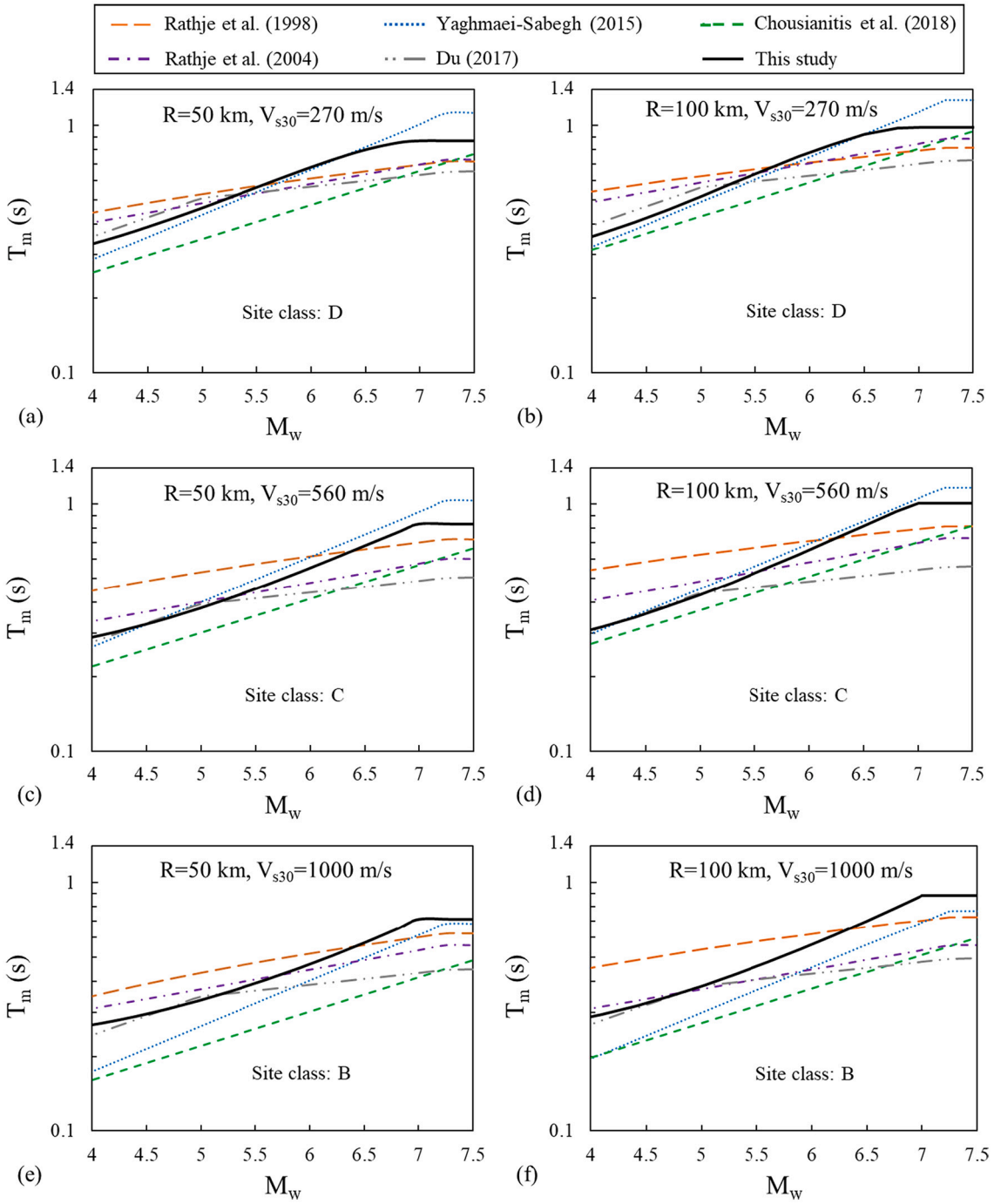

Fig. 14. Comparison of the values of T_m versus $M_w$predicted by the current model with the previous models for (a) Site class D,V_{s30} = 270 m/s, R = 50 km; (b) Site class D, V_{s30} = 270 m/s, R = 100 km; (c) Site class C, V_{s30} = 560 m/s, R = 50 km; (d) Site class C, V_{s30} = 560 m/s, R = 100 km; (e) Site class B, V_{s30} = 1000 m/s, R = 50 km; (f) Site class B, V_{s30} = 1000 m/s, R = 100 km.

provide a suitable perspective of the $T_m$estimation compared with Fig. 12, since they demonstrate the dependency of $T_m$on different parameters, such as M_w, R, and V_{s30}, concurrently. As shown in Fig. 12, the variations of contour lines of $T_m$values follow a gentle variation for low magnitudes. The variation of T_m increase for medium ($5 \leq M_w < 6$) and high ($6 \leq M_w < 7$) magnitudes. It was assumed constant for very high magnitude ($7 < M_w$). The comparison between the values of T_m indicates that it decreases from 0.77 to 0.59 for V_{s30} = 350 m/s and V_{s30} = 950 m/s, respectively, in R = 50 km and M_w = 6.5.

To the author's knowledge, a few empirical models have been proposed to predict T_m(Rathje et al., 1998; Rathje et al., 2004; Yaghmaei-Sabegh, 2015; Du, 2017; Chousianitis et al., 2018). The presented models by Rathje et al. (1998), Rathje et al. (2004), and Du (2017) were developed using the ground motion database of the worldwide earthquakes. The regional models were proposed by Yaghmaei-Sabegh (2015) and Chousianitis et al. (2018) for Iran and Greece, respectively. The properties of the models are outlined in Table 3.

As shown in Table 3, the predicted models are a function of different variables, while these parameters (R_{rup}, Z_{tor}, I_{dir}, Z_1, and FD) are not available for the available strong motion database of Iran. Hence, the effects of these variables (Z_{tor}, I_{dir}, Z_1, and FD) are ignored in the current comparative study. Moreover, the values of R_{rup} were not reported for

the Iranian input motion database and Ris used as the distance parameter of the recorded data. Accordingly, $R_{rup}$was assumed to be equal R in the models of Rathje et al. (1998), Rathje et al. (2004), Yaghmaei-Sabegh (2015), Du (2017). Moreover, the models of Rathje et al. (2004), Yaghmaei-Sabegh (2015), and Chousianitis et al. (2018) used an indicator variable (S_c and S_d) to designate site classes. Rathje et al. (1998)'s model was proposed for soil and rock sites. The models of Du (2017) and this study were developed based on the continuous V_{s30} parameter as a preferable site response variable for GMPEs (Kamai et al. 2014). The authors acknowledge the fact that some of the differences can be resulted in due to assumptions (e.g., distance, depth, and directivity), particularly for the models of Rathje et al. (1998), Rathje et al. (2004), Yaghmaei-Sabegh (2015), and Du (2017). The models proposed by Rathje et al. (1998), Rathje et al. (2004), and Du (2017) were developed based on the global ground motions with different tectonic characteristics. The current model, however, is a regional one, which was developed using the ground motion database of Iran. Hence, some of the differences between the models prediction can also be attributed to the source of data and regionalization of the dataset.

The predicted values of $T_m$by the models developed by Rathje et al. (1998), Rathje et al. (2004), Yaghmaei-Sabegh (2015), Du (2017), Chousianitis et al. (2018), and the current model (Eq. [9]) were plotted versus the variations of distance for $V_{s30} = 270$, 560 and 1000 m/sand $M_w = 5.5$ and 6.5 in Fig. 13. The values of V_{s30} were assigned as 270, 560, and 1000 m/s for site classes D, C, and B based on the average velocity in each site class. Fig. 13 indicates that the value of T_m is incrementally predicted for all site classes by all of the models when R increases. Figs. 13(a, c, and e) show that the current model provides a high value of $T_m$compared with the other models for $M_w = 6.5$. As shown in Figs. 13(b, d, and f), the current model predicts T_m in the middle range of other models. However, the difference between the current study and Yaghmaei-Sabegh (2015) is small for site classes D and C when $R > 50$.

Fig. 13 indicates that the presented model estimates different results compared with the Yaghmaei-Sabegh (2015)'s model as a regional model for Iran especially at $R < 50$ km for site classes D and C. However, they have a significant difference in site class B. The different strong motion database has potentially affected the fitting procedure as well as the selected functional form. As shown in Table 3, Yaghmaei-Sabegh (2015)'s model was developed using 575 records while the current model employed a larger database including 2281 earthquake records. The strong motion database used in the current model covers a wide range of site classes and magnitudes (see Fig. 2).

Fig. 14 illustrates the variations of the values of T_m versus M_w for different site classes predicted by the current model and the models developed by Rathje et al. (1998), Rathje et al. (2004), Yaghmaei-Sabegh (2015), Du (2017), and Chousianitis et al. (2018). Fig. 14 indicates that all the models follow an incremental trend when $M_w$increases. The model of Rathje et al. (1998) provides larger predictions for $M_w < 6$while the results of Chousianitis et al. (2018) is smaller for $M_w < 6.5$. The results of the current model are close the results of the models of Rathje et al. (2004) and Du (2017) for $M_w < 5.5$in all site classes. The predictive curves of this study are generally similar to the model of Yaghmaei-Sabegh (2015) for the site classes D, and C. However, difference between the current model and Yaghmaei-Sabegh (2015) is relatively high for site class B.

5. Conclusions

An empirical relationship has been proposed to predict the mean period of horizontal earthquake acceleration records using seismic events recorded in Iran. The empirical model was developed based on 4562 strong-motion records in Iran from 1975 to 2019. The model can be used to predict seismic behavior of engineering systems in Iran, especially regarding to landslides.

The presented model directly correlates T_m to earthquake magnitude M_w and source-to-site distance R. However, it was indirectly correlated toV_{s30}through a multiple regression analysis. The residuals of the predictive model were carefully examined for the possible undesired bias versus the input variables. It is shown that the residuals are at an acceptable level so that more than 65% of residuals fall between ±0.5(ln unit). A comparison between the results of the current and three predictive models confirmed that the current model was fitted well on the recorded data compared with the other models.

Declaration of Competing Interest

The authors declare that they have no known competing financial interests or personal relationships that could have appeared to influence the work reported in this paper.

Acknowledgments

The work described in the current study supported by Iran National Science Foundation (INSF) under Contract Number 99032044. This support is greatly appreciated. The authors would like to express their deep appreciation to Dr. Hamid Zafarani and Dr. Mohammad Reza Soghrat for their kind cooperation to modify the earthquake records. The authors thank Ms. Najme Alidadi who assisted the authors in data compilation.

Appendix A. Supplementary data

Supplementary data to this article can be found online at https://doi.org/10.1016/j.enggeo.2022.106526.

References

Allen, T.I., Wald, D.J., 2009. On the use of high-resolution topographic data as a proxy for seismic site conditions (VS 30). Bull. Seismol. Soc. Am. 99, 935–943.
Ansari, A., Noorzad, A., Zafarani, H., Vahidifard, H., 2010. Correction of highly noisy strong motion records using a modified wavelet de-noising method. Soil Dyn. Earthq. Eng. 30, 1168–1181.
Atkinson, G.M., Boore, D.M., 2007. Boore-Atkinson NGA Ground Motion Relations for the Geometric Mean Horizontal Component of Peak and Spectral Ground Motion Parameters. Pacific Earthquake Engineering Research Center.
Atkinson, G.M., Morrison, M., 2009. Observations on regional variability in ground-motion amplitudes for small-to-moderate earthquakes in North America. Bull. Seismol. Soc. Am. 99, 2393–2409.
Bastami, M., Soghrat, M., 2017. An empirical method to estimate fatalities caused by earthquakes: the case of the Ahar–Varzaghan earthquakes (Iran). Nat. Hazards 86, 125–149.
Berberian, M., 2014. Earthquakes and Coseismic Surface Faulting on the Iranian Plateau. Elsevier.
Bommer, J.J., Akkar, S., 2012. Consistent source-to-site distance metrics in ground-motion prediction equations and seismic source models for PSHA. Earthquake Spectra 28, 1–15.
Bourdeau, C., Havenith, H.-B., Fleurisson, J.-A., Grandjean, G., 2004. Numerical Modelling of Seismic Slope Stability. In: Hack, R., Azzam, R., Charlier, R. (Eds.), Engineering Geology for Infrastructure Planning in Europe: A European Perspective. Springer, Berlin Heidelberg, Berlin, Heidelberg, pp. 671–684.
Bravo-Haro, M.A., Elghazouli, A.Y., 2018. Influence of earthquake duration on the response of steel moment frames. Soil Dyn. Earthq. Eng. 115, 634–651.
Brune, J.N., 1970. Tectonic stress and the spectra of seismic shear waves from earthquakes. J. Geophys. Res. 75, 4997–5009.
Campbell, K.W., Bozorgnia, Y., 2007. Campbell-Bozorgnia NGA Ground Motion Relations for the Geometric Mean Horizontal Component of Peak and Spectral Ground Motion Parameters. Pacific Earthquake Engineering Research Center.
Castellaro, S., Mulargia, F., Rossi, P.L., 2008. VS30: Proxy for seismic amplification? Seismological Research Letters 79, 540–543.
Chiou, B., Youngs, R., Abrahamson, N., Addo, K., 2010. Ground-motion attenuation model for small-to-moderate shallow crustal earthquakes in California and its implications on regionalization of ground-motion prediction models. Earthquake Spectra 26, 907–926.
Chopra, A.K., 2001. Dynamics of Structures: Theory and Application to Earthquake Engineering. Prentice Hall Inc., Englewood Cliffs, NJ.
Chousianitis, K., Del Gaudio, V., Pierri, P., Tselentis, G.A., 2018. Regional ground-motion prediction equations for amplitude-, frequency response-, and duration-based parameters for G reece. Earthquake Engineering & Structural Dynamics 47, 2252–2274.
Del Gaudio, V., Pierri, P., Chousianitis, K., 2019. Influence of site response and focal mechanism on the performance of peak ground motion prediction equations for the Greek region. Soil Dyn. Earthq. Eng. 125, 105745.

Du, W., 2017. An empirical model for the mean period (T m) of ground motions using the NGA-West2 database. Bull. Earthq. Eng. 15, 2673–2693.
Du, W., 2019. Empirical correlations of frequency-content parameters of ground motions with other intensity measures. J. Earthq. Eng. 23, 1073–1091.
Farajpour, Z., Pezeshk, S., Zare, M., 2019. A New Empirical Ground-Motion Model for IranA New Empirical Ground-Motion Model for Iran. Bull. Seismol. Soc. Am. 109, 732–744.
Hickey, J., Broderick, B., 2019. Influence of mean period of ground motion on inelastic drift demands in cbfs designed to eurocode 8. Eng. Struct. 182, 172–184.
Jafarian, Y., Lashgari, A., 2016. Simplified procedure for coupled seismic sliding movement of slopes using displacement-based critical acceleration. International Journal of Geomechanics 16, 04015101.
Jafarian, Y., Lashgari, A., 2017. Seismic sliding analysis of sandy slopes subjected to pore-water pressure buildup. International Journal of Geomechanics 17, 04017106.
Jafarian, Y., Lashgari, A., Miraei, M., 2018. Multivariate fragility functions for seismic landslide hazard assessment. J. Earthq. Eng. 1–18.
Jafarian, Y., Lashgari, A., Haddad, A., 2019. Predictive Model and Probabilistic Assessment of Sliding Displacement for Regional Scale Seismic Landslide Hazard Estimation in Iran. Bull. Seismol. Soc. Am. 109, 1581–1593.
Jafarian, Y., Vakili, R., Abdollahi, A.S., Baziar, M.H., 2014. Simplified soil liquefaction assessment based on cumulative kinetic energy density: attenuation law and probabilistic analysis. Int. J. Geomech 14 (2), 267–281.
Jibson, R.W., Tanyaş, H., 2020. The influence of frequency and duration of seismic ground motion on the size of triggered landslides—A regional view. Eng. Geol. 273, 105671.
Karimi, Z., Dashti, S., 2017. Ground motion intensity measures to evaluate II: the performance of shallow-founded structures on liquefiable ground. Earthquake Spectra 33, 277–298.
Kotha, S.R., Cotton, F., Bindi, D., 2018. A new approach to site classification: Mixed-effects Ground Motion Prediction Equation with spectral clustering of site amplification functions. Soil Dyn. Earthq. Eng. 110, 318–329.
Kramer, S.L., 1996. Geotechnical Earthquake Engineering. Pearson Education India.
Kumar, M., Castro, J., Stafford, P., Elghazouli, A., 2011. Influence of the mean period of ground motion on the inelastic dynamic response of single and multi degree of freedom systems. Earthquake Engineering & Structural Dynamics 40, 237–256.
Lashgari, A., Jafarian, Y., Haddad, A., 2018. Predictive model for seismic sliding displacement of slopes based on a coupled stick-slip-rotation approach. Eng. Geol. 244, 25–40.
Lashgari, A., Jafarian, Y., Haddad, A., 2020. A coupled stick-slip-rotation model for earthquake-induced sliding displacement of slopes in Iran. Soil Dyn. Earthq. Eng. 135, 106199.
Lashgari, A., Jafarian, Y., Haddad, A., 2021. Predictive model for seismic sliding displacement of slopes subjected to pulse-like motions. Bull. Eng. Geol. Environ. 1–20.
Lin, P.-S., Lee, C.-T., Cheng, C.-T., Sung, C.-H., 2011. Response spectral attenuation relations for shallow crustal earthquakes in Taiwan. Eng. Geol. 121, 150–164.
Macedo, J., Candia, G., Lacour, M., Liu, C., 2020. New developments for the performance-based assessment of seismically-induced slope displacements. Eng. Geol. 277, 105786.
Rathje, E.M., Antonakos, G., 2011. A unified model for predicting earthquake-induced sliding displacements of rigid and flexible slopes. Eng. Geol. 122, 51–60.
Rathje, E.M., Bray, J.D., 1999. An examination of simplified earthquake-induced displacement procedures for earth structures. Can. Geotech. J. 36, 72–87.
Rathje, E.M., Abrahamson, N.A., Bray, J.D., 1998. Simplified frequency content estimates of earthquake ground motions. J. Geotech. Geoenviron. 124, 150–159.
Rathje, E.M., Faraj, F., Russell, S., Bray, J.D., 2004. Empirical relationships for frequency content parameters of earthquake ground motions. Earthquake Spectra 20, 119–144.
Rathje, E.M., Wang, Y., Stafford, P.J., Antonakos, G., Saygili, G., 2014. Probabilistic assessment of the seismic performance of earth slopes. Bull. Earthq. Eng. 12, 1071–1090.
Saygili, G., Rathje, E.M., 2008. Empirical predictive models for earthquake-induced sliding displacements of slopes. J. Geotech. Geoenviron. 134, 790–803.
Song, R., Li, Y., van de Lindt, J.W., 2014. Impact of earthquake ground motion characteristics on collapse risk of post-mainshock buildings considering aftershocks. Eng. Struct. 81, 349–361.
Tsai, C.-C., Chien, Y.-C., 2016. A general model for predicting the earthquake-induced displacements of shallow and deep slope failures. Eng. Geol. 206, 50–59.
Ulusay, R., Tuncay, E., Sonmez, H., Gokceoglu, C., 2004. An attenuation relationship based on Turkish strong motion data and iso-acceleration map of Turkey. Eng. Geol. 74, 265–291.
Wald, D.J., Allen, T.I., 2007. Topographic slope as a proxy for seismic site conditions and amplification. Bull. Seismol. Soc. Am. 97, 1379–1395.
Xu, Y., Wang, J., Wu, Y.-M., Kuo-Chen, H., 2019. Prediction models and seismic hazard assessment: A case study from Taiwan. Soil Dyn. Earthq. Eng. 122, 94–106.
Yaghmaei-Sabegh, S., 2015. New models for frequency content prediction of earthquake records based on Iranian ground-motion data. J. Seismol. 19, 831–848.
Zafarani, H., Soghrat, M., 2017. A selected dataset of the Iranian strong motion records. Nat. Hazards 86, 1307–1332.
Zafarani, H., Rahpeyma, S., Mousavi, M., 2017. Regional adjustment factors for three NGA-West2 ground-motion prediction equations to be applicable in northern Iran. J. Seismol. 21, 473–493.
Zafarani, H., Jafarian, Y., Eskandarinejad, A., Lashgari, A., Soghrat, M.R., Sharafi, H., Haji-Saraei, M.A.-e., 2020. Seismic hazard analysis and local site effect of the 2017 Mw 7.3 Sarpol-e Zahab, Iran, earthquake. In: Natural Hazards: Journal of the International Society for the Prevention and Mitigation of Natural Hazards, pp. 1–23.
Zhao, J.X., Zhou, S., Zhou, J., Zhao, C., Zhang, H., Zhang, Y., Gao, P., Lan, X., Rhoades, D., Fukushima, Y., 2016. Ground-motion prediction equations for shallow crustal and upper-mantle earthquakes in Japan using site class and simple geometric attenuation functions. Bull. Seismol. Soc. Am. 106, 1552–1569.